Surface & Coatings Technology 261 (2015) 149–155

Contents lists available at ScienceDirect

Surface & Coatings Technology

journal homepage: www.elsevier.com/locate/surfcoat

Effect of thermal annealing on the structural, electrical and optical properties of Al–Ni co-doped ZnO thin films prepared using a sol–gel method

X.L. Zhang [a], K.S. Hui [b,*], Feng Bin [c], K.N. Hui [a,**], Lei Li [a], Y.R. Cho [a], Rajaram S. Mane [d], Wei Zhou [e]

[a] School of Materials Science and Engineering, Pusan National University, San 30 Jangjeon-dong, Geumjeong-gu, Busan 609-735, Republic of Korea
[b] Department of Mechanical Convergence Engineering, Hanyang University, 17 Haengdang-dong, Seongdong-gu, Seoul 133-791, Republic of Korea
[c] State Key Laboratory of High-Temperature Gas Dynamics, Institute of Mechanics, Chinese Academy of Science, Beijing, PR China
[d] Centre for Nano-materials & Energy Devices, School of Physical Sciences, SRTM University, 431606 Nanded, India
[e] Department of Mechanical & Electrical Engineering, Xiamen University, Xiamen 361005, PR China

ARTICLE INFO

Article history:
Received 26 August 2014
Accepted in revised form 19 November 2014
Available online 22 November 2014

Keywords:
Al–Ni co-doped ZnO
Annealing temperature
Sol–gel method
Forming gas

ABSTRACT

Al–Ni co-doped ZnO (NiAl:ZnO) thin films were deposited on glass substrates using a sol–gel method. Based on a previous study, $Zn_{1-x}Al_xO$ (AZO; Al/Zn = 1.5 mol%) thin films optimized with a Ni content of 0.5 mol% were annealed at different temperatures from 450 to 600 °C in N_2/H_2 (95/5) forming gas for 1 h. The effects of the annealing temperature on the structural, electrical and optical properties were determined. X-ray diffraction showed that NiAl:ZnO thin film annealed at 500 °C exhibited the best crystallization quality. XPS revealed the presence of metallic Ni and Ni_2O_3 states, as well as Ni and Al atoms were successfully doped in NiAl:ZnO films, which did not result in a change in ZnO crystal structure and orientation. Scanning electron microscopy showed that the films were smooth and compact, and the grain size increased with increasing annealing temperature from ~23.8 nm to ~34.6 nm. According to the Hall Effect measurements, when the temperature reached 500 °C, the resistivity of the thin film showed the lowest value of 1.05×10^{-3} (Ω cm), which is the lowest resistivity reported for NiAl:ZnO films. The UV–Vis transmission spectra showed a high transmittance of more than 80% in the visible light range, and the band gap of the films was increased from 3.30 to 3.55 eV. This study showed that the annealing temperature in the forming gas is a vital factor affecting the quality of thin films. In addition, 500 °C was found to be the most appropriate annealing temperature for NiAl:ZnO films. This study provides a simple and efficient method for preparing high quality, high transparency and low resistivity NiAl:ZnO films for optoelectronic applications.

1. Introduction

Transparent conducting oxide (TCO) thin films are used widely in organic light-emitting diodes, solar cells, etc. [1,2]. Commercially available indium-tin oxide (ITO) has dominated the optoelectronic market because of its high transmittance in the visible region, very low resistivity and strong adhesion with glass [3]. However, ITO materials are expensive because of the scarcity of indium, and there is the issue of toxicity and low stability to H_2 plasma [4]. Thus by far, zinc oxide (ZnO) has been regarded as an alternative to ITO because of its enhanced electrical, optical, and mechanical properties [5–10], and is found to have potential in many optoelectronic applications [11,12]. In particular, Al-doped ZnO transparent conducting oxide thin films have been studied extensively in terms of their low cost and high conductivity [13]. On the other hand, ZnO films doped with magnetic metals, e.g., Fe [14], Co [15], and Ni [16], have been investigated widely for optoelectronic and magnetoelectronic applications. Li et al. [17] deposited Ni-doped ZnO:Al films on glass substrates by direct current (DC) magnetron co-sputtering at different deposition temperatures. The films grown at 473 K showed the lowest resistivity of 7.7×10^{-3} (Ω cm) and a mean optical transmittance of more than 90%. Later on, Jo et al. [18] reported on the deposited Al–Ni co-doped ZnO films with different Ni contents by DC magnetron sputtering in an argon atmosphere at room temperature and showed that the electrical resistivity of NiAl:ZnO films decreased to 2.59×10^{-3} (Ω cm) at a Ni doping concentration of 3 wt.%. In a similar study, Lee et al. [19] reported a low resistivity of 2.19×10^{-3} (Ω cm) of Al–Ni co-doped ZnO films with 5 wt.% Ni content by DC magnetron sputtering at room temperature at low sputtering power of 40 W. Most efforts reported previously require a sophisticated magnetron co-sputtering equipment, resulting in a relative high production cost. Therefore, alternative fabrication techniques should be explored to synthesize co-doped ZnO thin films.

* Corresponding author. Tel.: +82 2 2220 0441; fax: +82 2 2220 2299.
** Corresponding author. Tel.: +82 51 510 2467; fax: +82 51 514 4457.
E-mail addresses: kshui@hanyang.ac.kr (K.S. Hui), bizhui@pusan.ac.kr (K.N. Hui).

http://dx.doi.org/10.1016/j.surfcoat.2014.11.043
0257-8972/

In contrast, sol–gel method is an inexpensive, potentially large scale technique for preparing high quality thin films that allow uniform mixing at the molecular level. Recently, Li et al. [20] demonstrated a low resistivity of 2.07×10^{-3} (Ω cm) of Ni–Al co-doped ZnO (0.5 mol% Ni and 1.5 mol% Al) thin films by a cost-effective sol–gel method. Hui et al. [21] reported a low resistivity of 6.94×10^{-3} (Ω cm) of Cu–Al co-doped ZnO (0.5 mol% Cu and 1.5 mol% Al) thin films by a sol–gel method. However, few studies have examined the influence of the annealing temperature in N_2/H_2 forming gas on co-doped ZnO films, even though annealing treatment is a very important factor for optimizing the structural, optical, and electrical properties of thin films. In this study, Al–Ni co-doped ZnO (NiAl:ZnO) thin films were synthesized on glass substrates using a sol–gel method. The effect of thermal annealing from 450 to 600 °C in N_2/H_2 forming gas on the structural, electrical and optical properties of the NiAl:ZnO films was investigated in detail.

2. Experiment

In this study, zinc acetate dehydrate [$(C_2H_3O_2)_2$ Zn·$2H_2O$], aluminum nitrate nonahydrate [AlN_3O_9·$9H_2O$], nickel (II) chloride hexahydrate [Cl_2Ni·$6H_2O$], diethanolamine (DEA) [$C_4H_{11}NO_2$], and propylene glycol monoethyl ether (PGME) [$C_4H_{10}O_2$] were purchased from Sigma-Aldrich. All chemicals were of analytical grade and used as received.

The solution was prepared using a sol–gel method. First, 0.75 M of zinc acetate dehydrate was dissolved in PGME as a solvent. To extract a sufficient quantity of zinc acetate dihydrate, equal molar quantities of DEA, which act as a stabilizer, were mixed with PGME. The DEA zinc acetate dehydrate molar ratio was 1:1. The required amounts of aluminum nitrate nonahydrate and nickel (II) chloride hexahydrate to achieve an Al/Zn molar ratio of 1.5% and a Ni/Zn molar ratio of 0.5% were added to the solution. The mixture was then stirred for at least 12 h at room temperature, until a transparent precursor solution was formed.

To form the NiAl:ZnO thin film, the solution was coated by spin-coating at 3000 rpm for 30 s on a glass substrate (Corning glass E2000), which was cleaned sequentially with acetone, methanol and DI water in an ultrasonic bath. Subsequently, the thin films were placed on a hot plate at 160 °C for 10 min to dry the films, and then in a 400 °C furnace for 10 min in air to evaporate the solvent and remove the organic residues. The coating and drying processes were repeated 10 times. Finally, the derived thin films were annealed in N_2/H_2 (95/5) forming gas at different temperatures (450, 500, 550, and 600 °C) for 1 h. In this study, the film thickness of all films was determined to be approximately 400 nm using α-step method.

X-ray diffraction (XRD, Bruker AXS D8 Discover) using Cu-Kα was carried out to analyze the crystallinity and growth orientation of the as-obtained films. The Al/Zn and Ni/Zn compositions of the films on glass substrates were investigated by energy dispersive analysis of X-ray (EDX; HORIBA; 7593-H). X-ray photoelectron spectroscopy from KBSI (XPS, VG Scientifics ESCALAB250) was used to analyze the chemical bonding status of the NiAl:ZnO films. The surface morphology of the films was observed by field emission scanning electron microscopy (FESEM, HITACHI; S-4800). The electrical properties were characterized by Hall Effect measurements (HMS-3000, ECOPIA). The optical transmission measurements were confirmed by UV–Visible spectroscopy (HP 8453, Agilent). The spectral region used in this study was 200–1100 nm.

3. Results and discussion

Fig. 1 shows the XRD patterns of NiAl:ZnO thin films annealed at various annealing temperatures from 450 to 600 °C in N_2/H_2 (95/5) forming gas. Results showed that the NiAl:ZnO thin films have a polycrystalline hexagonal wurtzite structure that matched the

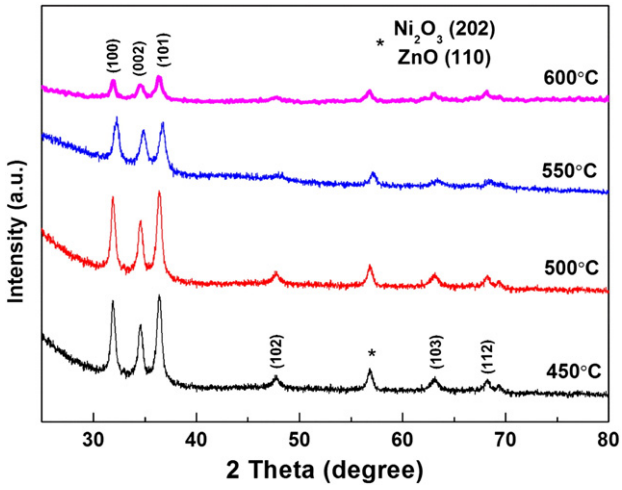

Fig. 1. XRD patterns of NiAl:ZnO thin films annealed at various annealing temperatures.

JCPDS file (no. 36-1451). The XRD peaks of the films at 31.7, 34.4, 36.2, 47.5, 56.6, 62.8, and 66.4° 2θ were assigned to the (1 0 0), (0 0 2), (1 0 1), (1 0 2), (1 1 0), (1 0 3) and (1 1 2) planes of hexagonal ZnO, respectively. Results indicated that Al and Ni dopants had no pronounced influence on the crystal structure of ZnO except for the presence of a polycrystalline Ni_2O_3 (202) phase at 56.7° 2θ, which agrees with a previous report [20]. On the other hand, the intensity of the three main diffraction peaks, such as (100), (002), and (101), first increased then decreased with increasing annealing temperature from 450 °C to 600 °C, suggesting that the crystallinity of the derived films improved initially and then deteriorates. The results showed that the (002) peak of the sample annealed at 500 °C was closest to the corresponding value of 34.422° 2θ for standard ZnO powders, as shown in Table 1. This variation was caused mainly by the stress generated in the doped ZnO thin films, which was expected due to the lattice mismatch with the guest element and thermal treatment. To explain this variation, the stress of the NiAl:ZnO thin films was obtained using following expressions, which are valid for a hexagonal lattice [22],

$$\text{stress} = \frac{2C_{13}^2 - C_{33}(C_{11}+C_{12})}{2C_{13}} \times \frac{C_{film} - C_{bulk}}{C_{bulk}} \quad (1)$$

where C_{11}, C_{22}, C_{13}, and C_{33} denote the elastic constants of ZnO film in different directions with the values of 208.8, 119.7, 104.2, and 213.8 GPa, respectively [22]. C_{bulk} is the lattice constant of standard ZnO power (C_{bulk} = 0.5205 nm) and C_{film} is the lattice constant of the deposited film in this experiment. Table 1 shows the calculated stress of the NiAl:ZnO thin films annealed at different temperatures. All the NiAl:ZnO films exhibited a positive stress showing that the stress was tensile. Tensile stress was observed when the annealing temperature reached 450 °C, which is due to the replacement of the Zn^{2+} (0.74 Å) by the guest elements, Al^{3+} (0.57 Å) and Ni^{2+} (0.69 Å), with a smaller radius [23]. With increasing annealing temperature to 500 °C, the tensile stress decreased because the impurity atoms could easily transfer from one unstable position to a stable and

Table 1
Experimental results at different annealing temperatures.

Annealing temperature (°C)	2θ of (002) peak(°)	FWHM of (002) peak (°)	Grain size (nm)	c = λ/sinθ(nm)	Stress(GPa)
450	34.558	0.3936	23.1	0.5184	0.9064
500	34.457	0.0984	27.8	0.5199	0.2469
550	34.677	0.4720	31.4	0.5168	1.6786
600	34.567	0.2458	33.5	0.5183	0.9651

equilibrium position, leading to the release of tensile stress. Further increasing the annealing temperature to 550 °C resulted in an increase in tensile stress, which was attributed to the different thermal expansion coefficients between the glass substrate and ZnO films [24]. However, as the annealing temperature increased to 600 °C, the stress decreased again. To explain this phenomenon, we should know that the total stress in the thin films mainly consisted of two components: (1) the intrinsic stress, which is introduced by the doping and defects during the growth, and (2) the extrinsic stress, which is introduced by the mismatch in lattice constants and thermal expansion coefficients between the thin films and substrates [4]. In our case, the intrinsic stress and extrinsic stress are competitive relation. When NiAl:ZnO film was annealed at 600 °C, the intrinsic stress was decreased due to the shift of atoms from non-equilibrium position to a more equilibrium position. On the contrary, the extrinsic stress was increased because of the difference in the thermal expansion coefficient of the ZnO and that of the glass substrate. In the case of NiAl:ZnO film annealed at 600 °C, the decrease in the stress is probably due to the release of intrinsic stress which was dominant compared with the extrinsic stress as compared with film annealed at 550 °C.

The Scherrer's equation [25] was used to calculate the mean grain size of the samples.

$$D = \frac{k\lambda}{\beta_D \cos\theta} \tag{2}$$

where k is a constant of 0.94, λ is the x-ray wavelength of 1.54 Å for CuK_α, θ is the Bragg diffraction angle, and β_D is the FWHM of θ. The transformed Eq. (2) can be expressed as follows:

$$\cos\theta = \frac{k\lambda}{D}\left(\frac{1}{\beta_D}\right). \tag{3}$$

The term, cos θ, was plotted with respect to (1/β) for the preferred orientation peaks of NiAl:ZnO thin films with the wurtzite hexagonal phase from 20° to 80° 2θ. By fitting the data, the grain size D was extracted from the slope of the linearly fitted line. The calculated grain sizes of the NiAl:ZnO thin films annealed at 450, 500, 550, and 600 °C were 23.1, 27.8, 31.4, and 33.5 nm, respectively (Table 1). The grain size increased with increasing annealing temperature to 600 °C due to the promotion of grain growth by the heat treatment. As the full width at half maximum (FWHM) is an indication of the crystallinity [9], the minimum FWHM of 0.0984° was observed for the sample annealed at 500 °C, suggesting that the film has a better crystallinity.

Fig. 2 shows SEM images of the NiAl:ZnO thin films prepared at various annealing temperatures in the forming gas. The microstructure of the films consisted of many round-shaped particles at annealing temperatures of 450 °C and 500 °C. At 450 °C, the film exhibited fine grains and the particle size was approximately 24.8 nm. At 500 °C, similar microstructure was observed on the film with the grain size of ~28.6 nm. When the annealing temperature was increased to 600 °C, the grains become larger (~33 nm for 550 °C, and 34.6 nm for 600 °C) and the surface become rougher. The growth in grain size resulted in a decrease in the grain boundary density, and inter-grain connections developed due to coarsening during coalescence, as shown in Fig. 2. Fig. 2(e) is a cross section SEM micrograph of NiAl:ZnO film annealed at 600 °C, showing a

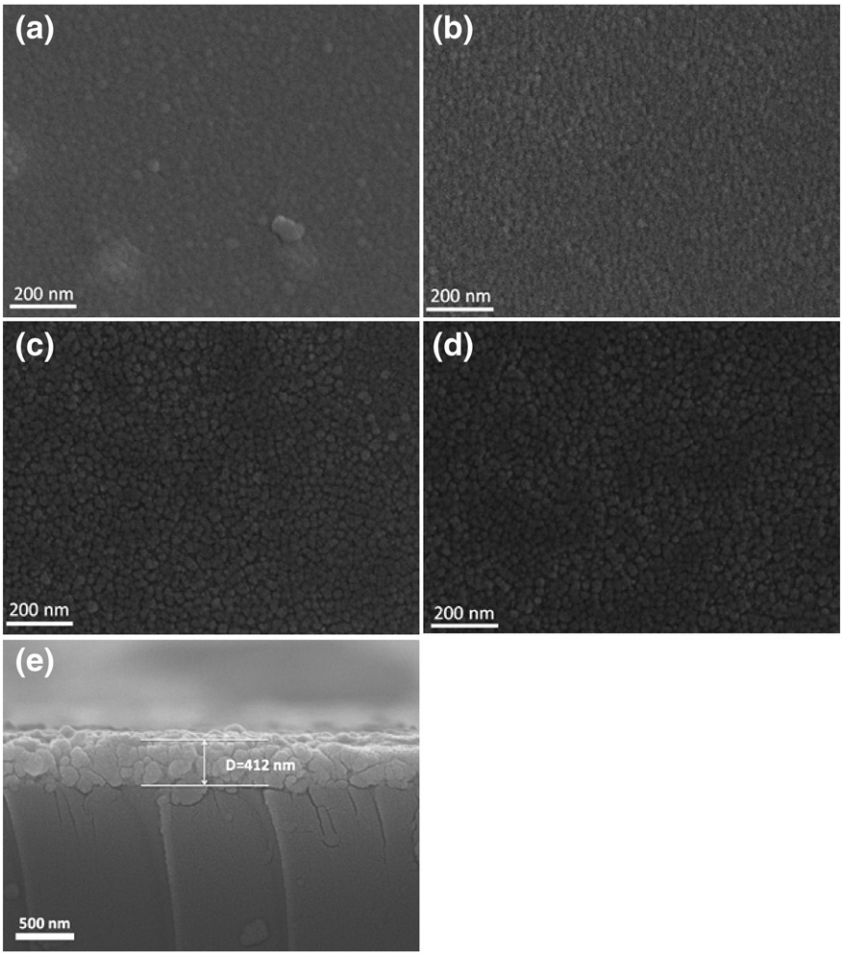

Fig. 2. SEM images of NiAl:ZnO thin films annealed at various annealing temperatures: (a) 450 °C, (b) 500 °C, (c) 550 °C, (d) 600 °C and (e) the cross section of (d).

film thickness of 412 nm, which is in good agreement with the value obtained from α-step method.

To further demonstrate the doping of Al and Ni atoms in the ZnO films, the XPS spectra in the Al 2p and Ni 2p regions for the NiAl:ZnO thin film annealed at 500 °C was measured. As shown in Fig. 3a, the binding energy of Al–O for Al 2p peak was clearly observed at 74.6 eV [26], indicating the doping of Al atoms in the ZnO films. On the other hand, the distinct asymmetry in Ni $2p_{3/2}$ photoelectron peaks was resolved into two components, one for metallic Ni and one for oxidized Ni, as shown in Fig. 3b. The XPS peak fitting of the $Ni2p_{3/2}$ (Ni metal) and $Ni2p_{3/2}$ (Ni_2O_3) peaks of the NiAl:ZnO thin films was located at approximately 852.5 eV [27] and 855.7 eV [28], respectively. These peaks confirm the existence of metallic Ni particles and Ni_2O_3 phase in the ZnO lattice. The formation of metallic Ni particles was attributed to the reduction of nickel oxide to metallic nickel particle in the N_2/H_2 annealing process [20], whereas the Ni_2O_3 phases can be explained by a weaker bond enthalpy of Zn–O (159 kJ mol^{-1}) than Ni–O (382 kJ mol^{-1}) such that Zn–O provides excess oxygen to the surrounding Ni atoms in the AZO matrix [29]. As a result, the excess oxygen in non-stoichiometric NiO_x will create Ni vacancies to occupy the Ni^{2+} sites [30], leading to the creation of Ni^{3+} ions and oxygen vacancies.

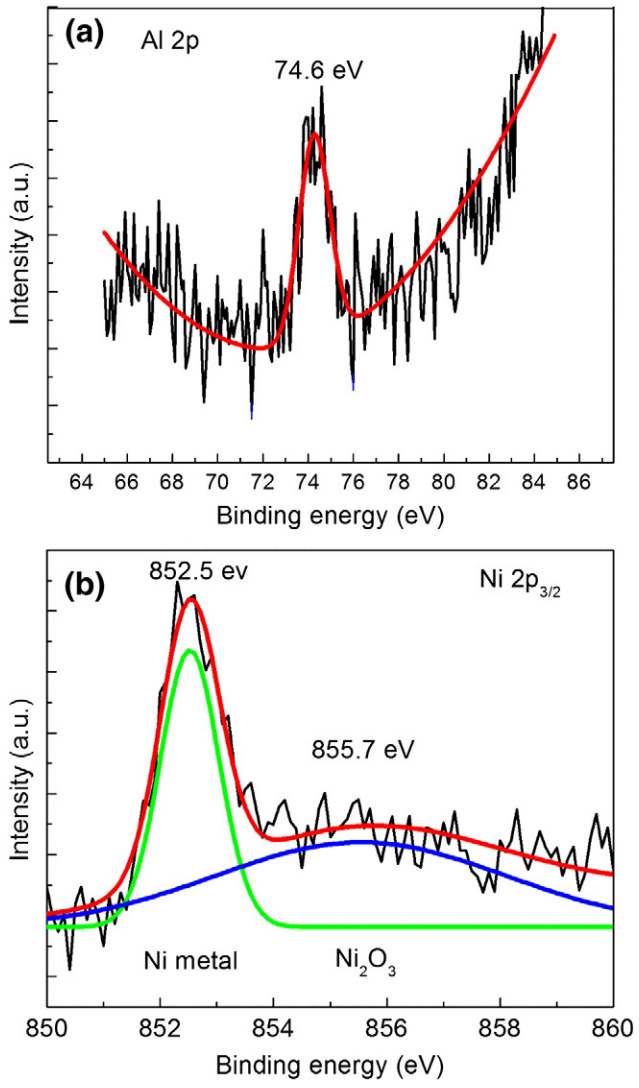

Fig. 3. XPS spectra in the (a) Al 2p and (b) Ni 2p regions of the NiAl:ZnO thin film annealed at 500 °C.

To investigate the effect of annealing temperature on the chemical bonding states of the NiAl:ZnO films, XPS of Zn 2p region of the NiAl:ZnO thin films annealed at 450, 500, and 550 °C was compared and shown in Fig. 4. The XPS spectra of all NiAl:ZnO films revealed symmetric peaks at ~1022.5 eV and ~1045.5 eV, corresponding to Zn $2p_{3/2}$ and Zn $2p_{1/2}$ states originating from Zn–O bonding located, respectively [31]. With increasing the annealing temperature to 550 °C, the intensities of the 2p peaks were decreased gradually. This is ascribed to the evaporation of Zn at higher temperature [32]. In addition, the binding energies of Zn $2p_{3/2}$ and Zn $2p_{1/2}$ states of the films match closely the ZnO standard values, suggesting that the oxidation state of Zn atoms is +2 in the NiAl:ZnO films.

Fig. 5 illustrated the O 1s XPS spectra of NiAl:ZnO films annealed at 450, 500, and 550 °C. Single peak around 531.5 eV corresponding to the oxygen vacancies (O_v) was observed [26]. The intensity of the O_v peak substantially decreased with increasing annealing temperature, suggesting the creation of significant density of oxygen vacancies with increasing annealing temperature in the N_2/H_2 treatment. This is because higher annealing temperature in N_2/H_2 forming gas facilitates the combination of H_2 with O atoms in the NiAl:ZnO films, resulting in an increase in oxygen vacancies.

Fig. 6 shows the charge mobility, charge carrier concentrations and electrical resistivity of NiAl:ZnO films with various annealing temperatures of 450, 500, 550, and 600 °C in N_2/H_2 forming gas. The highest carrier concentration of 2.15×10^{20} cm^{-3} with a mobility of 27.7 cm^2/V s was obtained at an annealing temperature of 500 °C (Table 2). With increasing annealing temperature from 450 to 500 °C, the films exhibited a larger grain size and higher charge carrier concentrations. The increase in carrier concentration was caused mainly by the generation of more oxygen vacancies in the ZnO matrix, and the gaseous reduction of NiO to Ni metal particle during thermal annealing under N_2/H_2 forming gas condition, which was confirmed by XPS analysis. In contrast, further increases in the annealing temperature to 550 °C, resulted in a decrease in carrier concentration. This was attributed to a decrease in the number of native donors because of the high vapor pressure of zinc, which resulted in the evaporation of Zn at higher temperatures [32], as evidence by the relative decrease in Zn 2p intensity (Fig. 4). On the other hand, the carrier mobility increased with increasing annealing temperature from 450 to 600 °C due to the increase of grain size, resulting in the decrease in electron scattering in grain boundaries [33]. Because the carrier concentration and mobility affect resistivity of the films, the annealing temperature in the forming gas plays an important role in controlling the electrical resistivity of the films. The electrical resistivity of NiAl:ZnO films decreased with increasing annealing temperature

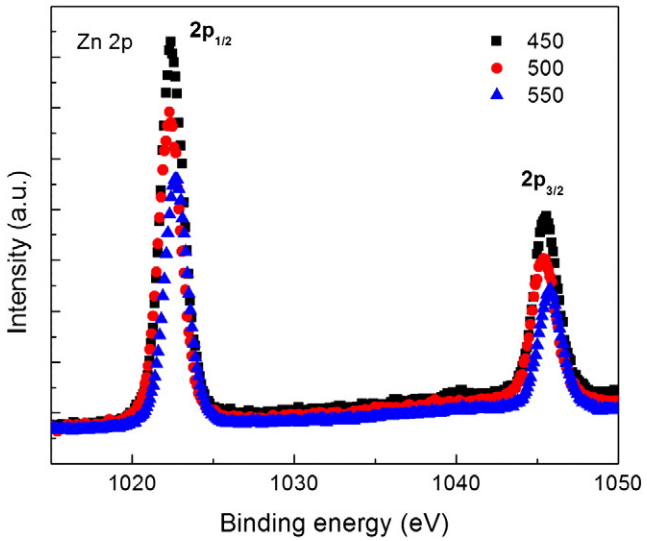

Fig. 4. XPS spectra of the Zn 2p of NiAl:ZnO thin films at different annealing temperatures.

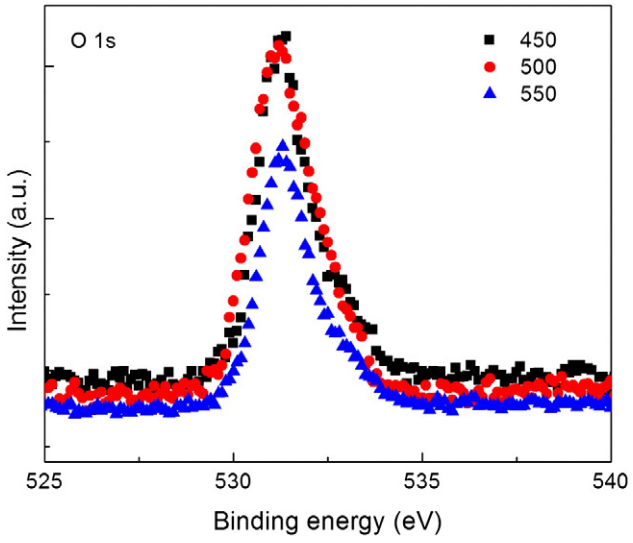

Fig. 5. XPS spectra of the O 1s of NiAl:ZnO thin films at different annealing temperatures.

from 450 to 500 °C, then increased with annealing temperature from 550 to 600 °C. The decrease in resistivity for the NiAl:ZnO thin films is attributed to both the increases in carrier concentration and mobility, which is ascribed by the formation of highly conductive Ni_2O_3 phases and the reduction of NiO to Ni in the N_2/H_2 annealing process, as well as the formation of a larger grain size. Nevertheless, when the heat treatment temperature gradually reached 600 °C, the crystal structure was degraded due to the mismatch of the coefficient of thermal expansion between the films and glass substrates, as shown in the XRD data (Fig. 1), resulting in high electrical resistivity.

High transparency is one of the most important factors for the application of ZnO thin films as TCOs. Fig. 7 presents the optical transmittance spectra with wavelengths from 200 to 1100 nm of the NiAl:ZnO films. All films showed a high average transmittance more than 80% and the transmittance decreased in the visible region with increasing annealing temperature from 450 to 600 °C. As SEM images revealed that the roughness of the NiAl:ZnO films increased with increasing the annealing temperature, the decrease in transmittance of the films at higher annealing temperature may due to the scattering effect from the rough surfaces. Tneh et al. [34] reported that surface roughness strongly affects the transmittance of ZnO based thin films. Sengupta et al. [35] showed the same trend for the decreasing transmittance of ZnO films with increasing annealing temperature from 400 to 700 °C. In addition, all NiAl:ZnO films exhibited interference fringes of the spectra with shallow valleys in the visible and near infrared regions due to an interference phenomenon between the top and bottom surfaces of the film [36]. Besides, the absorption edge was blue-shifted as the annealing temperature was increased. To explain this phenomenon, the band gap of the films was investigated. Fig. 8 shows the band gap estimated from the absorption edges of the samples annealed at different temperatures. The absorption edge for a direct interband transition can be estimated from the following equation:

Table 2
Electrical properties of NiAl:ZnO thin films at different annealing temperatures.

Annealing temperature (°C)	Al/Znratio	Ni/Znratio	Carrier concentration (cm^{-3})	Mobility (cm^2/Vs)	Resistivity (Ω cm)
450	0.89	0.26	5.19×10^{19}	23.6	5.09×10^{-3}
500	0.95	0.31	2.15×10^{20}	27.7	1.05×10^{-3}
550	0.97	0.31	1.05×10^{20}	28.7	2.07×10^{-3}
600	0.97	0.33	3.21×10^{19}	29.8	6.53×10^{-3}

$$\alpha h\nu = C\left(h\nu - E_g\right)^{1/2} \tag{4}$$

where C is a constant for a direct transition, and α is the optical absorption coefficient [25]. The optical energy gap, E_g, can then be obtained from the intercept of $(ahv)^2$ vs. hv for a direct transition. The energy bang gaps were obtained by extrapolating the linear absorption edge part of the curve using Eq. (4), as shown in Fig. 8. The band gaps of the samples increased with increasing annealing temperature from 450 to 600 °C, reaching a maximum of 3.55 eV at 600 °C. The band gaps of the NiAl:ZnO films are determined as 3.30, 3.31, 3.42, and 3.55 eV for 450, 500, 550 and 600 °C annealed samples, respectively. Dutta et al. [37] reported the observation of an increase in band gaps with an increase of ZnO grain size due to the less band bending at grain boundaries. In a similar study, Vinodkumar et al. [38] reported the enlargement of band gap with increase in grain sizes in Cd-doped ZnO films with increasing annealing temperature. In nanocrystalline, smaller grain sizes have a higher surface to volume ratios, which cause more band bending effect at the grain boundaries and the band edge becomes flatter than that of larger grains. Whereas in bigger grains, the band edge becomes sharper and band gap can be wider than that of smaller grains [39,40]. Therefore, the blue shift of band gaps of the NiAl:ZnO films can be attributed to the decrease in band bending effect at the grain boundaries, owing to the larger grain sizes with increasing annealing temperature (Table 1 and Fig. 2).

4. Conclusions

NiAl:ZnO thin films were fabricated on glass substrates at different annealing temperatures from 450 to 600 °C in a N_2/H_2 (95/5) forming

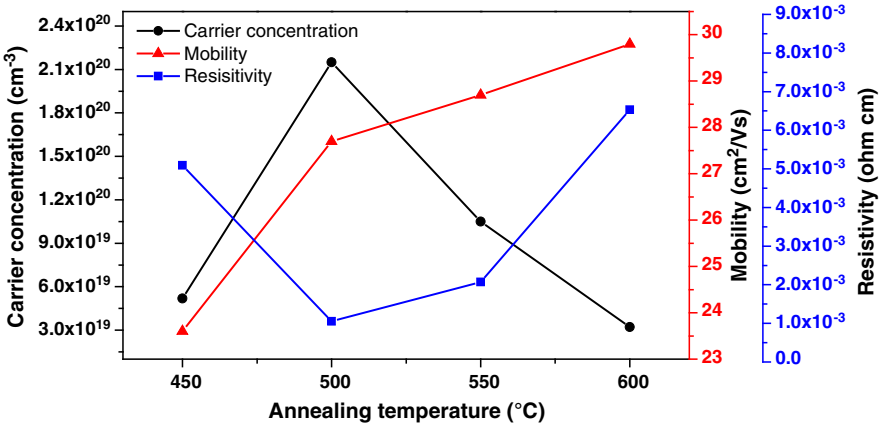

Fig. 6. Carrier concentration, mobility and resistivity of NiAl:ZnO thin films as a function of the annealing temperatures.

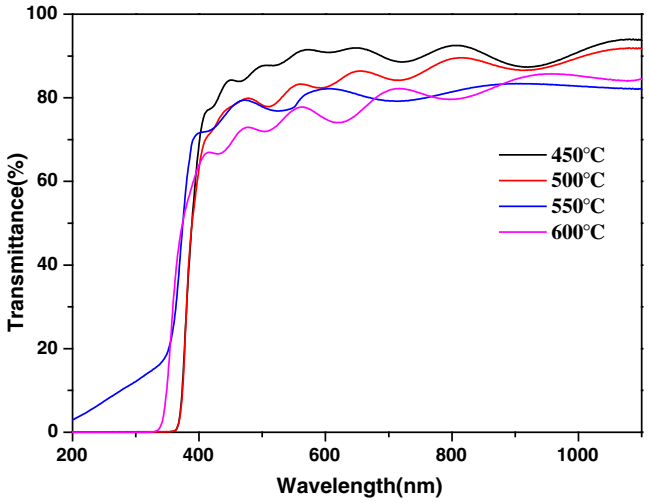

Fig. 7. Effect of the annealing temperature on the optical transmittance of NiAl:ZnO thin films.

gas using a sol–gel method. The intensity of the three main diffraction peaks of ZnO first increased, and then decreased with increasing annealing temperature from 450 to 600 °C, which suggests that the quality of NiAl:ZnO films is optimized at an annealing temperature of 500 °C. SEM showed that the grain size increased and the surface of films became rougher with increasing annealing temperature to 600 °C. XPS analysis revealed that Al and Ni atoms were successfully doped in ZnO lattices and the existence of metallic Ni and Ni_2O_3 states was observed in the NiAl:ZnO films. Increasing annealing temperature, the amount of oxygen vacancies was increased in the NiAl:ZnO films as evidence by XPS results. The resistivity of the thin films reached the lowest value of 1.05×10^{-3} (Ω cm) when the annealing temperature was 500 °C, which is the lowest resistivity for NiAl:ZnO reported thus far. In addition, all NiAl:ZnO films showed a high average transmittance of more than 80% in the range of the visible spectrum, and the band gaps of the films increased from 3.30 to 3.55 eV when the annealing temperature increased from 450 to 600 °C.

Acknowledgments

This work was supported by a 2-Year Research Grant of Pusan National University.

References

[1] D.C. Perng, J.W. Chen, T.T. Kao, R.P. Chang, Surf. Coat. Technol. 231 (2013) 261–266.
[2] W.C.H. Choy, K.N. Hui, H.H. Fong, Y.J. Liang, P.C. Chui, Thin Solid Films 509 (2006) 193–196.
[3] L.G. Ma, S.Y. Ma, H.X. Chen, X.Q. Ai, X.L. Huang, Appl. Surf. Sci. 257 (2011) 10036–10041.
[4] N.S. Kim, K.G. Yim, J.S. Son, J.Y. Leem, B. Korean Chem. Soc. 33 (2012) 1235–1241.
[5] D. Barreca, D. Bekermann, A. Devi, R.A. Fischer, A. Gasparotto, C. Maccato, E. Tondello, M. Rossi, S. Orlanducci, M.L. Terranova, Chem. Phys. Lett. 500 (2010) 287–290.
[6] D. Bekermann, A. Gasparotto, D. Barreca, A. Devi, R.A. Fischer, M. Kete, U.L. Stangar, O.I. Lebedev, C. Maccato, E. Tondello, G. Van Tendeloo, ChemPhysChem 11 (2010) 2337–2340.
[7] D. Barreca, A.P. Ferrucci, A. Gasparotto, C. Maccato, C. Maragno, E. Tondello, Chem. Vap. Depos. 13 (2007) 618–625.
[8] D. Barreca, A. Gasparotto, C. Maccato, E. Tondello, U.L. Stanger, S.R. Patil, Surf. Coat. Technol. 203 (2009) 2041–2045.
[9] X.L. Zhang, K.N. Hui, K.S. Hui, J. Singh, Mater. Res. Bull. 48 (2013) 1093–1098.
[10] J. Singh, P. Kumar, K.N. Hui, J. Jung, R.S. Tiwari, O.N. Srivasatva, Rsc. Adv. 3 (2013) 5465–5474.
[11] J. Singh, P. Kumar, D.J. Late, T. Singh, M.A. More, D.S. Joag, R.S. Tiwari, K.S. Hui, K.N. Hui, O.N. Srivastava, Dig. J. Nanomater. Biosci. 7 (2012) 795–806.
[12] X.L. Zhang, K.S. Hui, K.N. Hui, Mater. Res. Bull. 48 (2013) 305–309.
[13] T.F. Wei, Y.L. Zhang, Y. Yang, R.Q. Tan, P. Cui, W.J. Song, Surf. Coat. Technol. 221 (2013) 201–206.
[14] S.G. Protasova, B.B. Straumal, A.A. Mazilkin, S.V. Stakhanova, P.B. Straumal, B. Baretzky, J. Mater. Sci. 49 (2014) 4490–4498.
[15] Q. Xiao, T. Wang, Mater. Res. Bull. 48 (2013) 2786–2791.
[16] A.P. Rambu, L. Ursu, N. Iftimie, V. Nica, M. Dobromir, F. Iacomi, Appl. Surf. Sci. 280 (2013) 598–604.
[17] T.F. Li, H. Qiu, P. Wu, M.W. Wang, R.X. Ma, Thin Solid Films 515 (2007) 3905–3909.
[18] Y.D. Jo, K.N. Hui, K.S. Hui, Y.R. Cho, K.H. Kim, Mater. Res. Bull. 51 (2014) 345–350.
[19] J. Lee, K.N. Hui, K.S. Hui, Y.R. Cho, H.H. Chun, Appl. Surf. Sci. 293 (2014) 55–61.

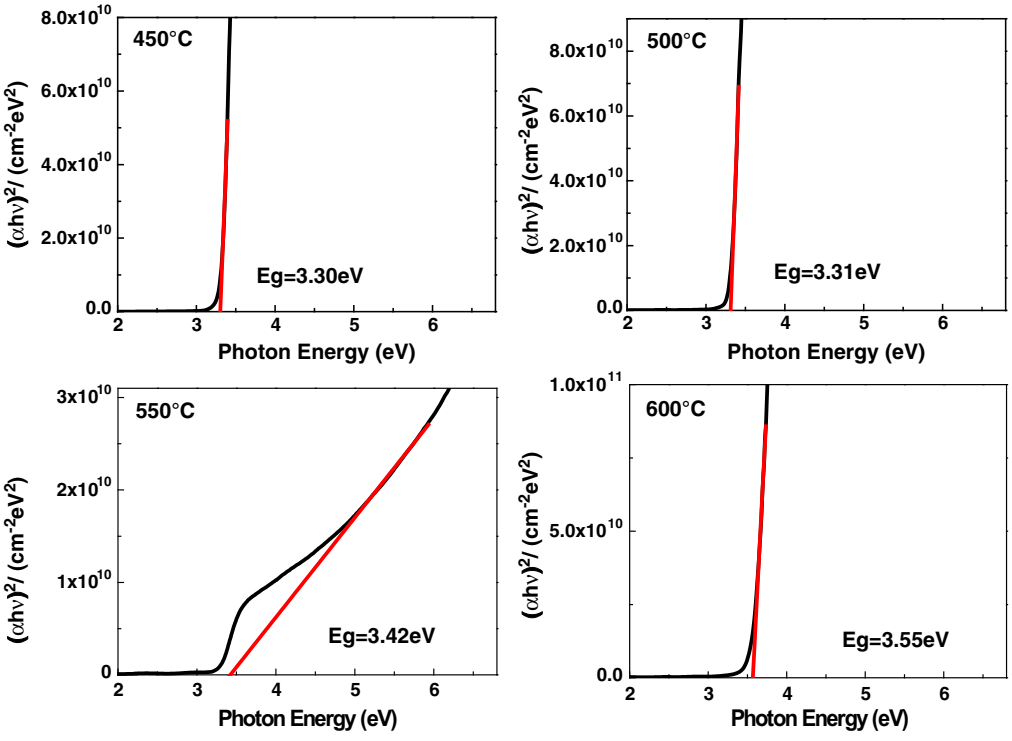

Fig. 8. Effect of the annealing temperature on the band gap of NiAl:ZnO thin films.

[20] L. Li, K.S. Hui, K.N. Hui, H.W. Park, D.H. Hwang, S. Cho, S.K. Lee, P.K. Song, Y.R. Cho, H. Lee, Y.G. Son, W. Zhou, Mater. Lett. 68 (2012) 283–286.
[21] K.N. Hui, K.S. Hui, L. Li, Y.R. Cho, J. Singh, Mater. Res. Bull. 48 (2013) 96–100.
[22] A. Singh, D. Kumar, P.K. Khanna, B.C. Joshi, M. Kumar, Appl. Surf. Sci. 258 (2011) 1881–1887.
[23] J.B.J. István Pais Jr., The Handbook of Trace Elements, St. Lucie Press, U.S.A, 1997.
[24] H. Wang, M.H. Xu, J.W. Xu, L. Yang, S.J. Zhou, J. Mater. Sci. Mater. 21 (2010) 145–148.
[25] S.Y. Kuo, W.C. Chen, F.I. Lai, C.P. Cheng, H.C. Kuo, S.C. Wang, W.F. Hsieh, J. Cryst. Growth 287 (2006) 78–84.
[26] X.Y. Zhang, J.Q. Qin, Y.N. Xue, P.F. Yu, B. Zhang, L.M. Wang, R.P. Liu, Sci. Rep. 4 (2014) 4596.
[27] K. Kishi, T. Fujita, Surf. Sci. 227 (1990) 107–113.
[28] K. Kishi, J. Electron Spectrosc. 46 (1988) 237–247.
[29] H.W. Park, J.H. Bang, K.N. Hui, P.K. Song, W.S. Cheong, B.S. Kang, Mater. Lett. 74 (2012) 30–32.
[30] K.K. Chattopadhyay, S. Nandy, B. Saha, M.K. Mitra, J. Mater. Sci. 42 (2007) 5766–5772.
[31] R.K. Singhal, S.C. Sharma, P. Kumari, S. Kumar, Y.T. Xing, U.P. Deshpande, T. Shripathi, E. Saitovitch, J. Appl. Phys. 109 (2011).
[32] H.W. Lee, S.P. Lau, Y.G. Wang, K.Y. Tse, H.H. Hng, B.K. Tay, J. Cryst. Growth 268 (2004) 596–601.
[33] J.P. Lin, J.M. Wu, Appl. Phys. Lett. 92 (2008) 134103.
[34] S.S. Tneh, Z. Hassan, K.G. Saw, F.K. Yam, H. Abu Hassan, Physica B 405 (2010) 2045–2048.
[35] J. Sengupta, R.K. Sahoo, K.K. Bardhan, C.D. Mukherjee, Mater. Lett. 65 (2011) 2572–2574.
[36] X.H. Wu, X.T. Hong, Z.P. Luo, K.S. Hui, H.Y. Chen, J.W. Wu, K.N. Hui, L.S. Li, J.M. Nan, Q.Y. Zhang, Electrochim. Acta 89 (2013) 400–406.
[37] S. Dutta, S. Chattopadhyay, M. Sutradhar, A. Sarkar, M. Chakrabarti, D. Sanyal, D. Jana, J. Phys. Condens. Matter 19 (2007) 236218.
[38] R. Vinodkumar, K.J. Lethy, P.R. Arunkumar, R.R. Krishnan, N.V. Pillai, V.P.M. Pillai, R. Philip, Mater. Chem. Phys. 121 (2010) 406–413.
[39] G. Li, X.B. Zhu, X.W. Tang, W.H. Song, Z.R. Yang, J.M. Dai, Y.P. Sun, X. Pan, S.Y. Dai, J. Alloys Compd. 509 (2011) 4816–4823.
[40] V. Srikant, D.R. Clarke, J. Appl. Phys. 81 (1997) 6357–6364.